RSC Advances

RSC Publishing

PAPER

View Article Online
View Journal | View Issue

Cite this: *RSC Advances*, 2013, **3**, 17411

Phase behavior of hierarchical mesoporous silicas prepared using ABC triblock copolymers as single templates†

Jheng-Guang Li, Ruei-Bin Lin and Shiao-Wei Kuo*

Received 16th April 2013,
Accepted 23rd July 2013

DOI: 10.1039/c3ra41814f

www.rsc.org/advances

In this study we found that complicated mesostructures featuring bimodal mesopore distributions could be fabricated through simple evaporation-induced self-assembly when employing lab-made poly(ethylene-*b*-ethylene oxide-*b*-ε-caprolactone) (PE-PEO-PCL) triblock copolymers as single templates without any other additives. Using this approach, we produced two kinds of ultra-complicated hierarchical mesoporous silica samples as a result of the unusual composition of the ABC-type triblock copolymer: hydrophobic segments at the termini and a hydrophilic segment in the middle. Notably, by adjusting the amount of tetraethyl orthosilicate (TEOS) in the reaction medium, we obtained a series of silica samples with well-defined morphologies and two types of well-ordered hierarchical mesostructures, namely ''alternate body-centered cubic'' and ''tetragonal cylinder alternated with face-centered cubic.'' Using small-angle X-ray spectroscopy, transmission electron microscopy, and isothermal N_2 adsorption–desorption experiments, we studied the phase behavior of the mesoporous silica samples templated by a series of PE-PEO-PCL triblock copolymers at various TEOS-to-PE-PEO-PCL-to-HCl weight ratios. Notably, we report the first example of the fabrication and characterization of the special ''alternate body-centered cubic'' mesostructure (E1T40).

Introduction

Hierarchical mesoporous nanostructures have received considerable attention because of their specific structures and unusual properties;[1–23] moreover, the hierarchical morphology of pore shapes or pore size distributions can also affect the functions of these materials in, for example, catalysis,[4,7,19] electrochemical capacitors,[5] sensing,[8] low refractive index materials,[11] and delivery.[12,16] The International Union of Pure and Applied Chemistry (IUPAC) defines a pore size of less than 2 nm as a ''micropore'', between 2 and 50 nm as a ''mesopore'', and of greater than 50 nm as a ''macropore''. Most hierarchical mesoporous materials contain two kinds of pore sizes–a so-called bimodal pore size distribution; commonly, hierarchical mesoporous materials feature a combination of micropores and mesopores or a combination of mesopores and macropores. Several synthetic methods have been reported for the fabrication of hierarchical porous structures, including opal and polymeric bead templating,[17] sacrificial polymeric nanoparticle templating,[1,2,6,8,11,14] controlled phase separation,[9,16] direct surfactant templating,[19] template-free fabrication,[7] and mesoporous (hierarchical) particle assembly.[3,20] Commonly, two kinds of surfactants have been used as templates to coordinate the formation of ordered structures,[1,2,4,6,12,22] co-solvents[23] have been added to induce pores of different length scales, and polymeric beads (including organic or inorganic species) have been added during the self-assembly process[1–3,6,8,11,14] to achieve the goal of hierarchical mesoporous morphologies.

The self-assembly of hierarchical nanostructures from ABC triblock copolymers has been an active area of research in recent years because they can form three-phase lamellae,[24] core/shell cylinders,[24,25] and other hierarchical structures.[26,27] The use of an ABC-type triblock copolymer as a template to prepare mesoporous materials was first reported by the Zhao group that synthesized highly ordered mesoporous carbons with large mesopores and tunable mesopore walls through an evaporation-induced self-assembly (EISA) strategy with a poly(ethylene oxide-*b*-methyl methacrylate-*b*-styrene) (PEO-PMMA-PS) triblock copolymer as the template and resol phenolic resin as the carbon source.[28] In their approach, the hydrophilic segment, PEO, was located at the chain end and the two hydrophobic segments, PMMA and PS, were connected; such a sequence distribution would lead to the production of only one type of mesoporous structure after calcination. The interconnected hydrophobic segments such as PMMA and PS could only cause single hydrophobic domain after the microphase separation of block copolymers (or so-

Department of Materials and Optoelectronic Science, National Sun Yat-Sen University, Kaohsiung, 804, Taiwan. E-mail: kuosw@faculty.nsysu.edu.tw

† Electronic supplementary information (ESI) available. See DOI: 10.1039/c3ra41814f

called self-assembly), as we know, the mesopores were mainly induced by the hydrophobic part of block copolymers, therefore, the ABC triblock copolymer with hydrophilic-hydrophobic–hydrophobic arrangement is only capable to fabricate the mesoporous material with single pore size distribution. That is why our template PE-PEO-PCL is so special from other ABC block copolymers as a template for the preparation of mesoporous materials; compared with other methods that were used for the preparation of hierarchical mesoporous silicas, our method is a breakthrough by using single template without any additives (cosolvent, contemplate or additional nanopartilces) for the first time.

In a previous paper, we reported the use of the amphiphilic ABC-type triblock copolymer poly(ethylene-*b*-ethylene oxide-*b*-ε-caprolactone) (PE-PEO-PCL, $E_{13}EO_{42}CL_{31}$) as a single template for fabricating hierarchical mesoporous silicas featuring two differently sized sets of mesopores.[21] In this study, we synthesized a series of PE-PEO-PCL copolymers of four different molecular weights–$E_{13}EO_{42}CL_9$, $E_{13}EO_{42}CL_{18}$, $E_{13}EO_{42}CL_{31}$, and $E_{13}EO_{42}CL_{44}$–and used them to fabricate hierarchical mesoporous silicas. The key issue when fabricating hierarchical mesoporous materials is how to produce, control, and order the hierarchical morphologies; here, we synthesized a series of hierarchical mesoporous silicas featuring various mesophases by regulating the tetraethyl orthosilicate (TEOS)-to-PE-PEO-PCL weight ratio, the molecular weight of the PCL segment in the PE-PEO-PCL triblock copolymer, and the HCl-to-PE-PEO-PCL ratio at a constant content of TEOS.

We investigated the phase behavior of these materials through small-angle X-ray scattering (SAXS), transmission electron microscopy (TEM), and isothermal N_2 adsorption–desorption [Brunauer–Emmett–Teller (BET)] experiments. Among the fabricated mesoporous silica samples, we found two interesting and complicated hierarchical nanostructures: mesoporous silicas (template: $E_{13}EO_{42}CL_9$) with ''alternate body-centered cubic'' structures and mesoporous silicas (template: $E_{13}EO_{42}CL_{31}$) with ''tetragonal cylinder alternated with face-centered cubic'' structures. In the former, the mesopores with simple cubic structures resulted from the PCL segments and the body-centered cubic (*BCC*) mesopores originated from the PE segments after calcination; in the latter, the tetragonal cylindrical mesopores resulted from the PCL segments and the *FCC* mesopores originated from the PE segments after calcination. In other words, when we changed the template from $E_{13}EO_{42}CL_9$ to $E_{13}EO_{42}CL_{31}$ (*i.e.*, varied the volume fractions of the PCL blocks in the PE-PEO-PCL triblock copolymer), the PE blocks transferred from the *BCC* substructure to *FCC* substructure in the hierarchical mesophase, and the PCL blocks changed the morphology from a simple cubic substructure to a tetragonal cylinder substructure. To the best of our knowledge, this paper reports the first systematic study of hierarchical mesoporous materials with bimodal pore size distributions (two kinds of mesopores) prepared in one pot using a single ABC triblock copolymer templating strategy. In the future, this strategy could give us a new version, to apply to the other ABC triblock copolymers, such as PS-PEO-PMMA, as the template for preparation of nanoarchitectonics for further applications,[29] for example, controlled drug delivery,[30] biomedical applications[31] and other applications.

Experimental

Materials

ε-Caprolactone (ε-CL, Acros) was purified through vacuum distillation over CaH_2; the distillation fraction collected at 96–98 °C (5 mm-Hg) was used in all polymerization reactions. Stannous(II) octoate [$Sn(Oct)_2$, Sigma] was used as received. Hexane, CH_2Cl_2, tetrahydrofuran (THF), TEOS, $HCl_{(aq)}$, and PE-PEO (M_n = 2250 g mol^{-1}; PEO 80 wt%) were used as received from Aldrich. Deionized water was employed in all experiments.

PE-PEO-PCL copolymers of various molecular weights[21]. Triblock copolymers were readily prepared through ring opening polymerization (ROP) of ε-CL with PE-PEO diblock copolymer as the macroinitiator in the presence of $Sn(Oct)_2$ as the catalyst (Scheme 1). The reaction mixtures were prepared by placing a desired weight of ε-CL monomer in a silanized flask containing a pre-weighed amount of PE-PEO under a N_2 atmosphere. Several drops of $Sn(Oct)_2$ were added and then the flask was connected to a vacuum line, evacuated, sealed off, and heated at 130 °C. After 24 h, the resulting block copolymers were dissolved in CH_2Cl_2 and precipitated in an excess of cold *n*-hexane. The triblock copolymers were dried at 40 °C under vacuum; their characterization data are listed in Table 1.

Mesoporous silicas templated by PE-PEO-PCL copolymers[32]. Mesoporous silicas were prepared through an EISA strategy in THF, using various copolymers ($E_{13}EO_{42}CL_9$, $E_{13}EO_{42}CL_{18}$, $E_{13}EO_{42}CL_{31}$ and $E_{13}EO_{42}CL_{44}$) as templates and TEOS as the silica precursor (Scheme 1). Various TEOS-to-PE-PEO-PCL weight ratios at a constant $HCl_{(aq)}$ concentration [0.1 g of 0.1 M $HCl_{(aq)}$ in 5 g of THF] or TEOS-to-PE-PEO-PCL-to-$HCl_{(aq)}$ weight ratios at a constant TEOS content (Table 2) were used; TEOS was added into a THF (5 g) solution of the block copolymer (2.0 wt%, containing 0.10 g of copolymer), with stirring, which was continued for 30 min to form a homogeneous solution. The sample was poured into a Petri dish and the THF was evaporated at room temperature for 48 h. The transparent film was collected and ground into a powder, which was then transferred to a PFA bottle containing 1.0 M HCl (30 mL) and treated hydrothermally at 100 °C for 3 days. The product was washed with water and EtOH, dried at room temperature, and calcined in air at 600 °C for 6 h to produce a white mesoporous silica. Calcination processes were conducted in a furnace operated at a heating rate of 1 °C min^{-1}.

Characterization

^1H NMR spectra were recorded at room temperature using a Bruker AM 500 (500 MHz) spectrometer, with the residual proton resonance of the deuterated solvent acting as the

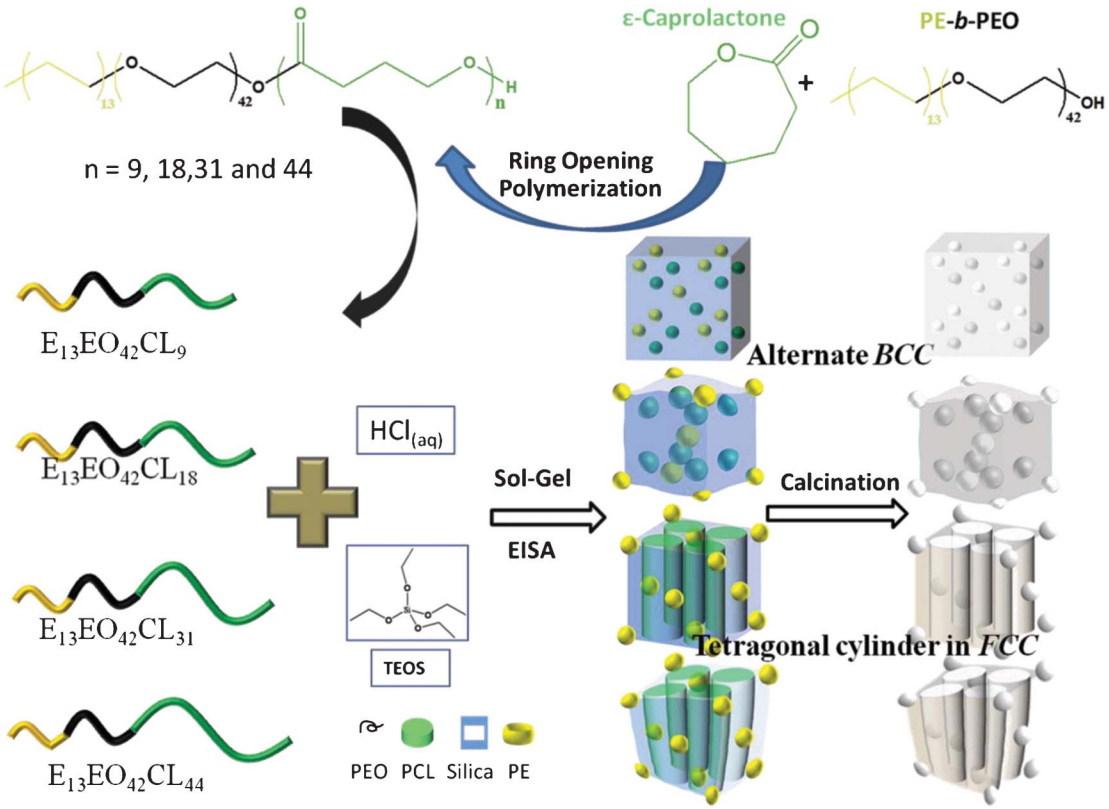

Scheme 1 Synthesis of PE-PEO-PCL triblock copolymers through ROP and preparation of hierarchical mesoporous silicas through EISA.

internal standard. Molecular weights were determined through gel permeation chromatography (GPC) using a Waters 510 high-performance liquid chromatograph equipped with a 410 differential refractometer and three Ultrastyragel columns (100, 500, and 10^3 Å) connected in series, with dimethylformamide (DMF) as the eluent (flow rate: 0.4 mL min^{-1}). SAXS experiments were performed using the SWAXS instrument at the BL17B3 beamline of the NSRRC, Taiwan. The X-ray beam had a diameter of 0.5 mm and a wavelength (λ) of 1.24 Å. The *d*-spacings were calculated using the formula $d = 2\pi/q$, where q is the scattering vector. TEM images were recorded using a JEOL 3010 microscope operated at 200 kV; samples for TEM measurement were suspended in EtOH and supported onto a holey carbon film on a Cu grid. Nitrogen adsorption–desorption isotherms were measured at −196 °C using an ASAP 2020 analyzer; prior to measurements, the samples were degassed under vacuum at 200 °C for at least 6 h. The BET method was used to calculate the specific surface areas and pore volumes; pore size distributions were derived from the adsorption branches of the isotherms by using the Barrett–Joyner–Halenda (BJH) model.

Table 1 Characterization data of PE-PEO-PCL triblock copolymers used in this study

Triblock Copolymer	M_n (^{1}H NMR)	M_n (GPC)	M_w (GPC)	PDI
$E_{13}EO_{42}CL_9$ (EEC1)	3276	7.6×10^3	9.8×10^3	1.19
$E_{13}EO_{42}CL_{18}$ (EEC2)	4302	1.03×10^4	1.23×10^4	1.29
$E_{13}EO_{42}CL_{31}$ (EEC3)	5784	1.54×10^4	1.76×10^4	1.14
$E_{13}EO_{42}CL_{44}$ (EEC4)	7266	1.95×10^4	2.93×10^4	1.50

Results and Discussion

Characterization of PE-PEO-PCL copolymers

To study the phase behavior of various mesoporous silicas templated by unique ABC type triblock copolymers PE-PEO-PCL, we prepared four different PE-PEO-PCL templates of high molecular weight through simple ROP using a commercial PE-PEO block copolymer ($E_{13}EO_{42}$; M_n = 2250 g mol^{-1}; PEO 80 wt%) as the macroinitiator, $Sn(Oct)_2$ as the catalyst, and THF as the solvent. GPC revealed a narrow polydispersity index (PDI, Fig. 1, Table 1) for each triblock copolymer; number-average molecular weights (M_n) were determined from ^{1}H NMR spectra by comparing their peak intensities with those of the commercial macroinitiator PE-PEO (Fig. 2, Table 1); self-assembly structure of four different PE-PEO-PCL templates (Fig. S1, ESI†). The PE-PEO-PCL triblock copolymers has the specific compositions as shown in Table 1.

Mesoporous silicas prepared using $E_{13}EO_{42}CL_9$ as template; alternate BCC hierarchical nanostructure

We used a simple EISA method to synthesize original mesoporous silica having an alternate *BCC* hierarchical nanostructure when applying $E_{13}EO_{42}CL_9$ (EEC1), a copolymer

Table 2 Textural properties of mesoporous silica samples templated by PE-PEO-PCL at various TEOS-to-PE-PEO-PCL ratios

Sample	d (nm)	Pore size (nm)	S_{BET} (m^2 g^{-1})	S_M (m^2 g^{-1})	Pore volume (cm^3 g^{-1})	Micropore volume (cm^3 g^{-1})	TEOS/$E_{13}EO_{42}CL_9$
E1T25	13.5	4.8; 7.5	581	84	0.73	0.033	2.5 : 1
E1T30	12.8	4.8	587	102	0.67	0.042	3 : 1
E1T35	12.6	4.8	795	182	0.82	0.078	3.5 : 1
E1T40	12.6	4.8	564	132	0.55	0.057	4 : 1
E1T45	12.6	4.8	492	103	0.48	0.044	4.5 : 1
							TEOS/$E_{13}EO_{42}CL_{18}$
E2T25	14.6	4.8; 8.6	493	64	0.74	0.025	2.5 : 1
E2T30	14.3	4.8; 9.6	545	118	0.71	0.05	3 : 1
E2T35	13.9	4.8	478	99	0.6	0.042	3.5 : 1
E2T40	13.4	4.8	486	120	0.56	0.052	4 : 1
E2T45	13.8	4.8	497	133	0.55	0.058	4.5 : 1
							TEOS/$E_{13}EO_{42}CL_{31}$
E3T25	15.7	3.8; 9.8	389	56	0.65	0.021	2.5 : 1
E3T30	14.1	3.8; 8.6	350	47	0.57	0.02	3 : 1
E3T35	14	3.8; 8.6	588	88	0.91	0.035	3.5 : 1
E3T40	14.1	3.8; 7.5	477	144	0.6	0.063	4 : 1
E3T45	13.5	3.8; 8.6	251	34	0.37	0.013	4.5 : 1
							TEOS/$E_{13}EO_{42}CL_{44}$
E4T25	20.6	4.3; 15.8	514	168	0.77	0.075	2.5 : 1
E4T30	21	3.8; 13.9	433	117	0.6	0.051	3 : 1
E4T35	21	4.8; 15.6	485	202	0.69	0.091	3.5 : 1
E4T40	21	4.8; 15.6	450	184	0.65	0.083	4 : 1
E4T45	20.5	4.8; 15.6	225	51	0.45	0.022	4.5 : 1

having a volume fraction of its CL block segment lower than those the other three PE-PEO-PCL copolymers, as the template at a TEOS-to-$E_{13}EO_{42}CL_9$ ratio of 4 : 1. The unusual arrangement of the three blocks in the PE-PEO-PCL copolymers (with the hydrophobic segments situated at the termini) resulted in a particular hierarchical structure–alternate *BCC*–after the EISA process; presumably, the central PEO block was surrounded by the silica precursors in the reaction medium and led to the formation of the silica walls, the terminal PE block was responsible for the mesopores having the *BCC* arrangement, and the terminal PCL block produced another *BCC* mesophase (Scheme 1, Fig. 3), in other words, it is *BCC* structure with two crystallographic sites, one kind of cage occupied (0, 0, 0) and another cage occupied (1/4, 1/4, 1/4).

We used SAXS, TEM, and BET isotherms to identify the structure of the hierarchical mesoporous silica templated by $E_{13}EO_{42}CL_9$. The SAXS pattern (Fig. 3a) of this hierarchical mesoporous silica (E1T40) exhibited two strong reflections with two large d-spacings of 12.56 and 8.88 nm, which we attribute to the primary and the second peaks of the alternate *BCC*, respectively; this SAXS pattern could be indexed as having (110) and (200) reflections, corresponding to a *BCC* structure. Fig. 3b illustrated the foreseeable hierarchical morphology of E1T40, as shown in Fig. 3b, the yellow balls

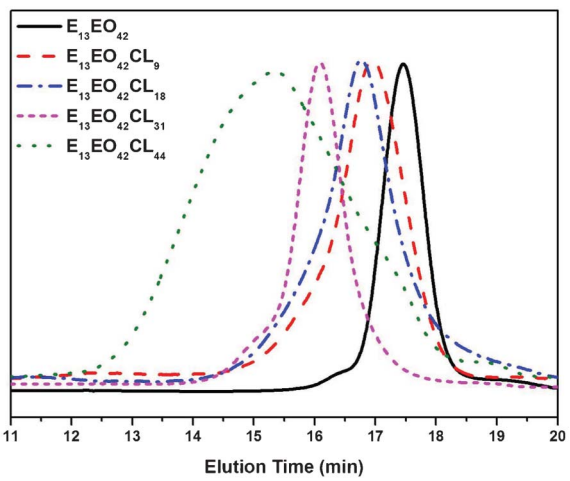

Fig. 1 GPC traces of the diblock copolymer $E_{13}EO_{42}$ (black line) and the triblock copolymers $E_{13}EO_{42}CL_9$ (red dashed line), $E_{13}EO_{42}CL_{18}$ (blue dashed line), $E_{13}EO_{42}CL_{31}$ (magenta dashed line), and $E_{13}EO_{42}CL_{44}$ (green dashed line).

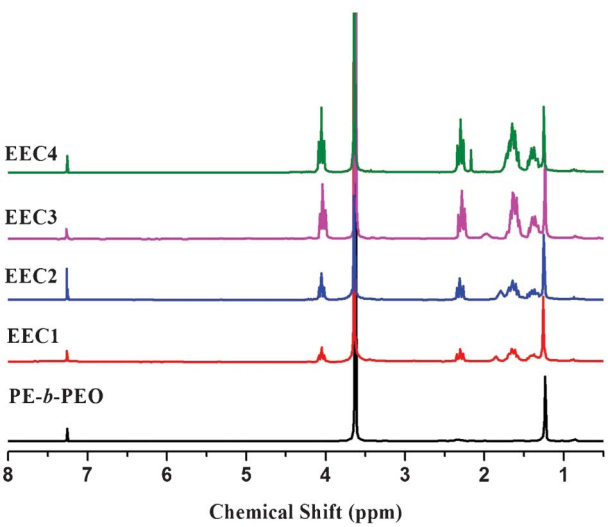

Fig. 2 ^1H NMR spectra of the copolymers PE-PEO and PE-PEO-PCL in $CDCl_3$.

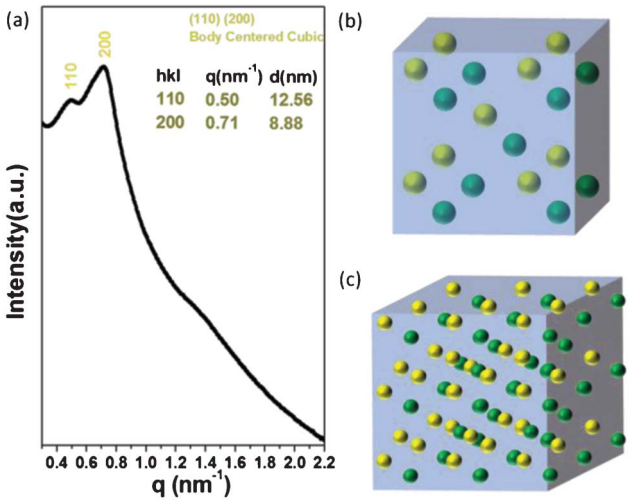

Fig. 3 (a) SAXS pattern, (b) (c) 3D model of ''alternate *BCC*'' hierarchical mesoporous silica templated by $E_{13}EO_{42}CL_9$ at a TEOS-to-$E_{13}EO_{42}CL_9$ ratio of 4 : 1.

represented the *BCC* structure, could be attributed the contribution of PE segment the other hand, the green balls displayed another *BCC* morphology inside the alternate *BCC* structure, resulted from the PCL segment (Fig. 3b). When we expand the alternate *BCC* structure to further repeat unit, a hierarchical mesostructure with several alternate *BCC* arrangements could be observed (Fig. 3c).

TEM images (Fig. 4a–c), their fast Fourier transform (FFT) (Fig. 4d–f) and corresponding diagrams (Fig. 4g–i) of the hierarchical mesoporous silica (E1T40) with different orientations ([100], [110], and [210] planes, respectively) were consistent with a three-dimensional (3D) complicated ''alternate *BCC* structure'' having the same *d*-spacing. Combination of the TEM images, corresponding FFT and foreseeable diagrams viewed from [100] (Fig. 4a, 4d and 4g), [110] (Fig. 4b, 4e and 4h) and [210] (Fig. 4c, 4f and 4i) direction, the unique alternate tetragonal, alternate rectangular and alternate parallelogram patterns could be observed along [100], [110] and [210], respectively. Those data give the powerful evidence of special hierarchical structure ''alternate *BCC*'' characters, more TEM images and tilt TEM images of hierarchical mesoporous silica with ''alternate *BCC*'' morphology (E1T40) could be obtained in Fig. S2 and S3, ESI.† We suspect that such a material might have practicality in storage and separation applications. Table 2 collected the textual properties of mesoporous silica sample E1T40 with ''alternate *BCC*'' morphology, as we know, the complicated structure composed of two kinds of substructures (one kind of cage occupied (0, 0, 0) and another cage occupied (1/4, 1/4, 1/4), respectively), and hence the textural properties of separate substructure were also listed in Table 2.

Fig. 5a displays the typical type-IV adsorption–desorption curve of the E1T40 sample, based on the IUPAC classification. It features two overlapping hysteresis loops, suggesting a hierarchical structure with two types of pores, but with similar pore size distributions (Fig. 5a). Sharp capillary condensation steps appeared for this sample, suggesting uniform pore dimensions and high-quality ordering of the materials, in agreement with the TEM and SAXS data. We used the Broekhoff–de Boer (BdB) model (with the assumption of spherical pores) to determine the pore sizes. Fig. 5b reveals that the single pore size distribution did, in fact, comprise two sorts of pores, contributed by the PE and PCL segments, respectively. The BET surface area of the samples was 564 m^2 g^{-1}; the pore volume was approximately 0.55 cm^3 g^{-1} (Table 2, E1T40).

For the shortest template $E_{13}EO_{42}CL_9$, indeed, the molecular weights of PE segment is higher than PCL segment, nevertheless, the pore size of the mesopore is not only decided by

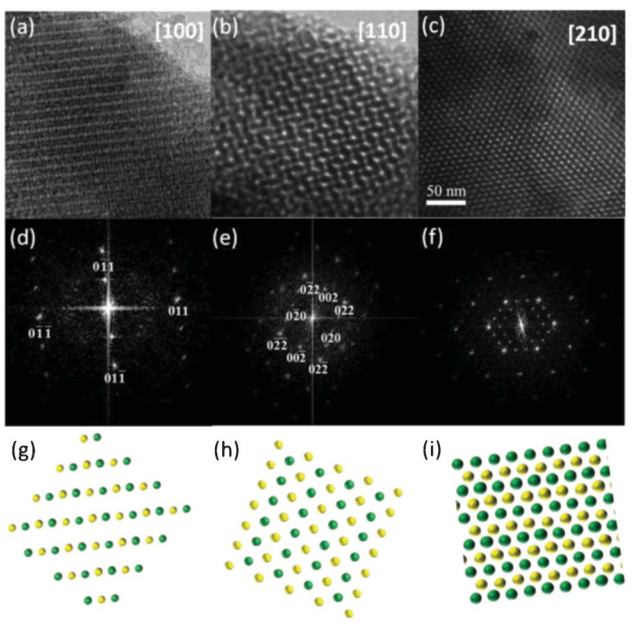

Fig. 4 TEM images (4a–c), corresponding FFT (4d–f) and the foreseeable diagrams (4g–i) of the ''alternate *BCC*'' mesoporous silica viewed from the [100] (4a, 4d and 4g), [110] (4b, 4e and 4h), and [210] (4c, 4f and 4i) planes, respectively.

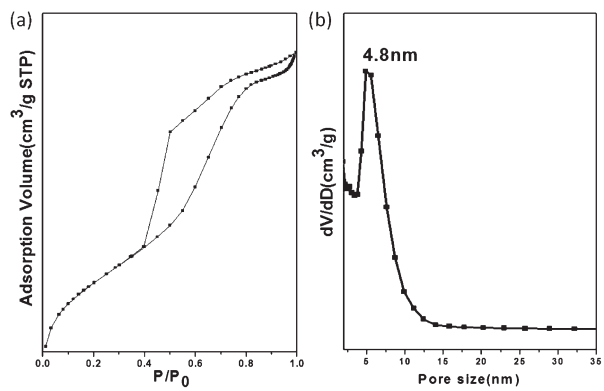

Fig. 5 (a) N_2 adsorption–desorption isotherm, and (b) pore size distribution curve of the ''alternate *BCC*'' mesoporous silica templated by $E_{13}EO_{42}CL_9$ at a TEOS-to-$E_{13}EO_{42}CL_9$ ratio of 4 : 1.

the molecular weight of each hydrophobic segment, but also be determined by the density of each domain, in other words, the volume of each domain is as the result of combination of many effects, such as the arranged ordering of each polymer segment chain and the properties of individual segment. Besides, we provide various hierarchical mesoporous silica samples on the basis of various conditions, we observed that the original structure of PCL is cylindrical structure (sample E3T40, template $E_{13}EO_{42}CL_{31}$) and the volume fraction reasonably decreased upon the molecular weight reduction of PCL segment till $E_{13}EO_{42}CL_9$, at the viewpoint of segment volume fraction we could reasonably conclude the structure of PCL domain would tend to sphere (E1T40) from cylinder (E3T40) with the volume fraction decrease of PCL domain.

We know the mesopores that originated from PE and PCL could have similar pore size even if the molecular weight of each segment is different. Based on this reason, we could see the pore size distributions of mesoporous silicas templated by different templates ($E_{13}EO_{42}CL_9$, $E_{13}EO_{42}CL_{18}$, $E_{13}EO_{42}CL_{31}$, and $E_{13}EO_{42}CL_{44}$, respectively) gradually transferred from bimodal to unimodal distribution with the molecular weight decrease of PCL segment. In addition, our pore size distributions are all calculated from the adsorption branch of isotherm N_2 sorption curves.

Mesoporous silicas templated by various PE-PEO-PCL copolymers at different TEOS-to-PE-PEO-PCL weight ratios

To further understand the phase behavior of the hierarchical mesoporous silicas templated by the unusual ABC-type triblock copolymers PE-PEO-PCL, we used TEM, SAXS, and BET analysis to identify and characterize a series of mesoporous silicas prepared at various TEOS-to-PE-PEO-PCL weight ratios, with the four PE-PEO-PCL copolymers ($E_{13}EO_{42}CL_9$, $E_{13}EO_{42}CL_{18}$, $E_{13}EO_{42}CL_{31}$, $E_{13}EO_{42}CL_{44}$) as templates.

First, we discuss the mesoporous silica samples templated by $E_{13}EO_{42}CL_9$ at TEOS-to-$E_{13}EO_{42}CL_9$ ratios of 2.5 : 1 (E1T25), 3 : 1 (E1T30), 3.5 : 1 (E1T35), 4 : 1 (E1T40), and 4.5 : 1 (E1T45). Fig. 6a displays TEM images of all of these samples, revealing similar "alternate *BCC*" hierarchical mesostructures. For the mesoporous silica samples prepared at higher TEOS-to-$E_{13}EO_{42}CL_9$ weight ratios (E1T30 to E1T45), the TEM images indicate the complex, ordered hierarchical mesostructures; for E1T25, however, the order of mesophase was lower and two spherical mesopores with different pore sizes were evident. The same phenomenon also appeared in the SAXS analysis (Fig. 6b). Again, all of the samples exhibited "Alternate *BCC*" hierarchical mesostructures. The second reflection peak of the *BCC* structures overlapped with the another reflection peak of the complicated structures; they could be indexes as reflec-

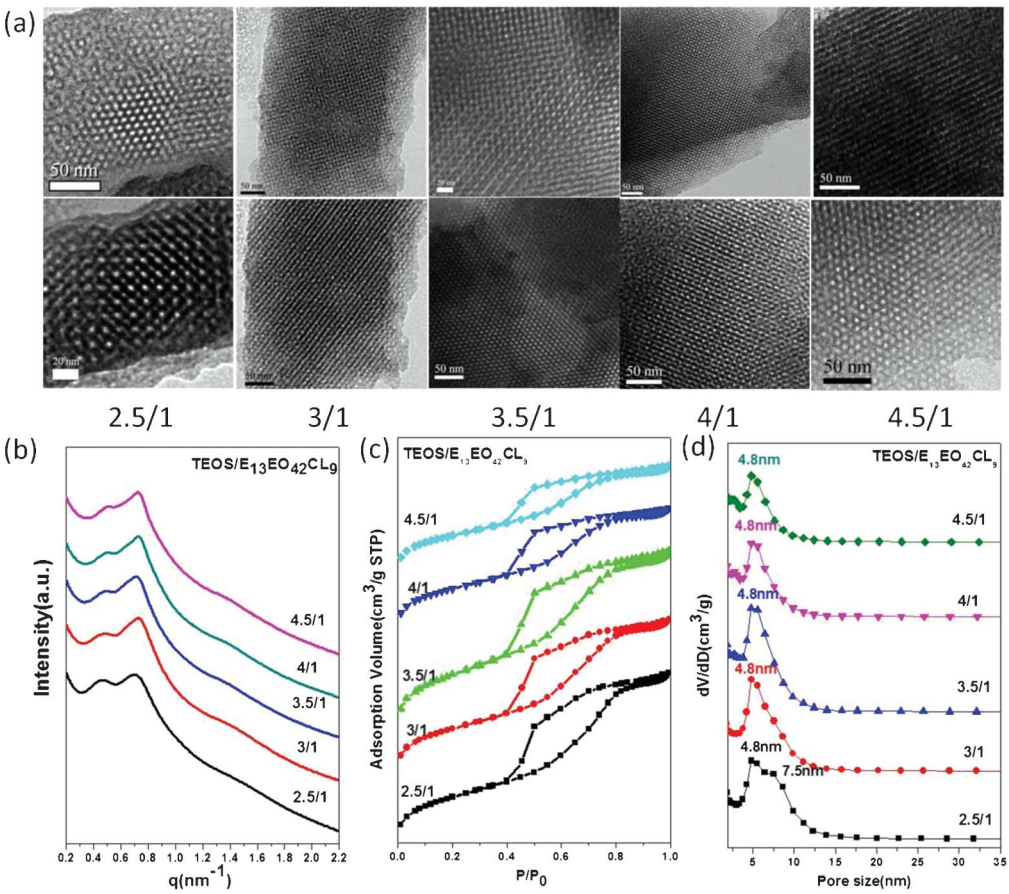

Fig. 6 (a) TEM images, (b) SAXS patterns, (c) N_2 adsorption–desorption isotherms, and (d) pore size distribution curves of mesoporous silicas templated by $E_{13}EO_{42}CL_9$ at TEOS-to-$E_{13}EO_{42}CL_9$ weight fractions of 2.5 : 1, 3.0 : 1, 3.5 : 1, 4 : 1, and 4.5 : 1.

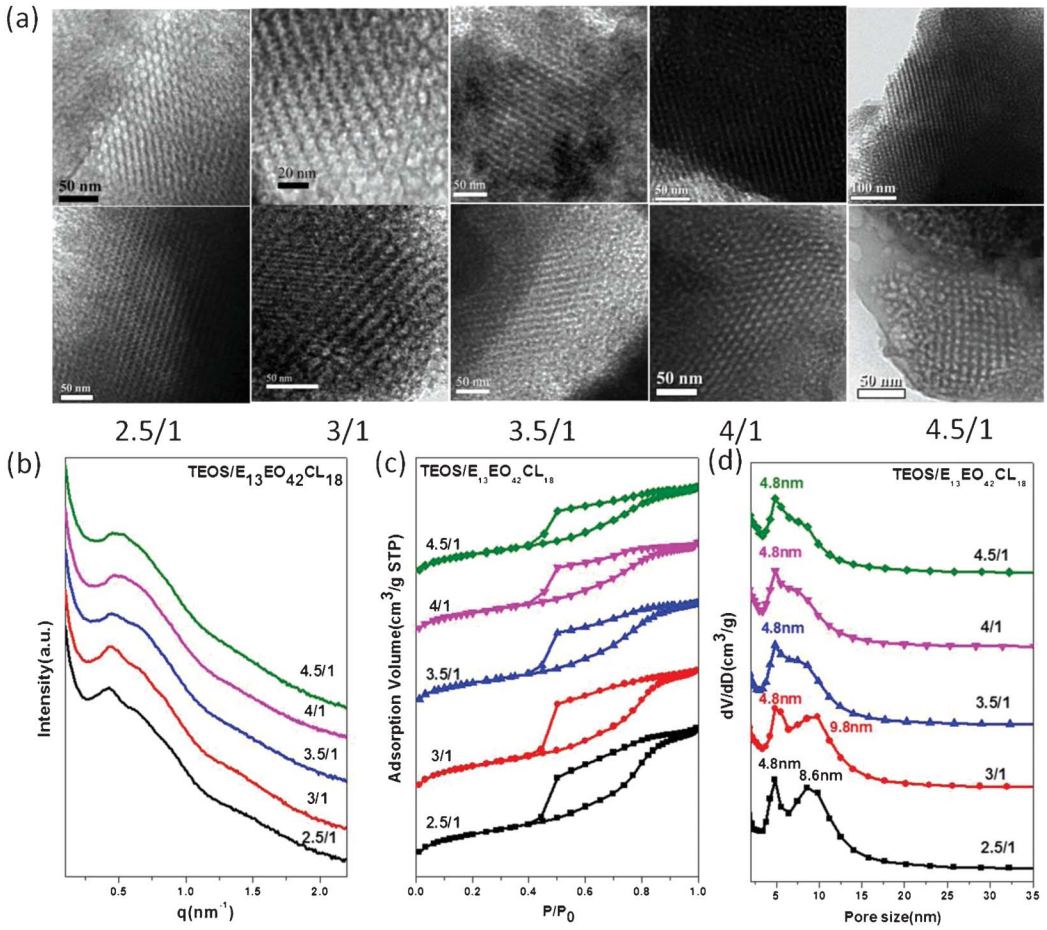

Fig. 7 (a) TEM images, (b) SAXS patterns, (c) N_2 adsorption–desorption isotherms, and (d) pore size distribution curves of mesoporous silicas templated by $E_{13}EO_{42}CL_{18}$ at TEOS-to-$E_{13}EO_{42}CL_{18}$ weight fractions of 2.5 : 1, 3.0 : 1, 3.5 : 1, 4 : 1, and 4.5 : 1.

tions of (200) and (100) planes, respectively. Notably, however, the SAXS pattern also indicated poorer order at the lower TEOS-to-$E_{13}EO_{42}CL_9$ weight ratio (E1T25). Fig. 6d presents the N_2 sorption curves and representative type-IV curves with capillary condensation steps in the relative pressure range from 0.55 to 0.80. All of these mesoporous silica samples templated by $E_{13}EO_{42}CL_9$ exhibited hybrid H_2-like hysteresis loops, characteristic of spherical mesopores. Based on the BdB model, we determined the mean pore size for the mesoporous silica samples E1T30 to E1T45, measured from their adsorption branches, to be 4.8 nm; in contrast, sample E1T25 exhibited an indistinct bimodal pore size distribution. Table 2 summarizes the primary *d*-spacings, surface areas, pore volumes, and pore sizes of these samples.

Next, we discuss the hierarchical mesoporous silica samples (E2T25 to E2T45) templated by $E_{13}EO_{42}CL_{18}$ (EEC2). From TEM, SAXS, and BET measurements (Fig. 7a–d), we found that the self-assembled mesostructures formed by the template $E_{13}EO_{42}CL_{18}$ (with its longer PCL segment) were more disordered than those templated by $E_{13}EO_{42}CL_9$, due to its mesophase being between two ordered hierarchical mesostructures (''alternate *BCC*'' and ''tetragonal cylinder alternated with *FCC*''). This finding means that the volume fraction of the hydrophobic PCL block in EEC2 was between those of $E_{13}EO_{42}CL_9$ (EEC1) and $E_{13}EO_{42}CL_{31}$ (EEC3) and that the mesophases of samples E2T25 to E2T45 were located in the disordered area of the silica/PE-PEO-PCL phase diagram. Fig. 7a displays TEM images of the mesoporous silica samples E2T25 to E2T45; although it was difficult to analyze their structures because they were not sufficiently ordered enough, we could still distinguish slight differences among them: the pore sizes of the mesoporous silica samples were larger when the TEOS-to-template weight fractions was low. Similarly, the SAXS patterns were also difficult to analyze, but they were different for each mesoporous silica sample (Fig. 7b), implying that the morphology changed depending on the TEOS-to-template weight fraction. Fig. 7c displays the N_2 adsorption–desorption curves of these samples; although mixed H_2-like hysteresis loops appeared in the relative pressure range from 0.5 to 0.8 $cm^3\ g^{-1}$, it remained difficult to distinguish the two separate hysteresis loops. Fig. 7d presents the pore size distributions of these mesoporous silica samples. The pore sizes tended toward bimodal distributions upon decreasing the TEOS-to-template weight fraction; in other words, the mesophase tended toward a sphere (resulting from PE segments) in sphere (resulting from PCL segments) hierarch-

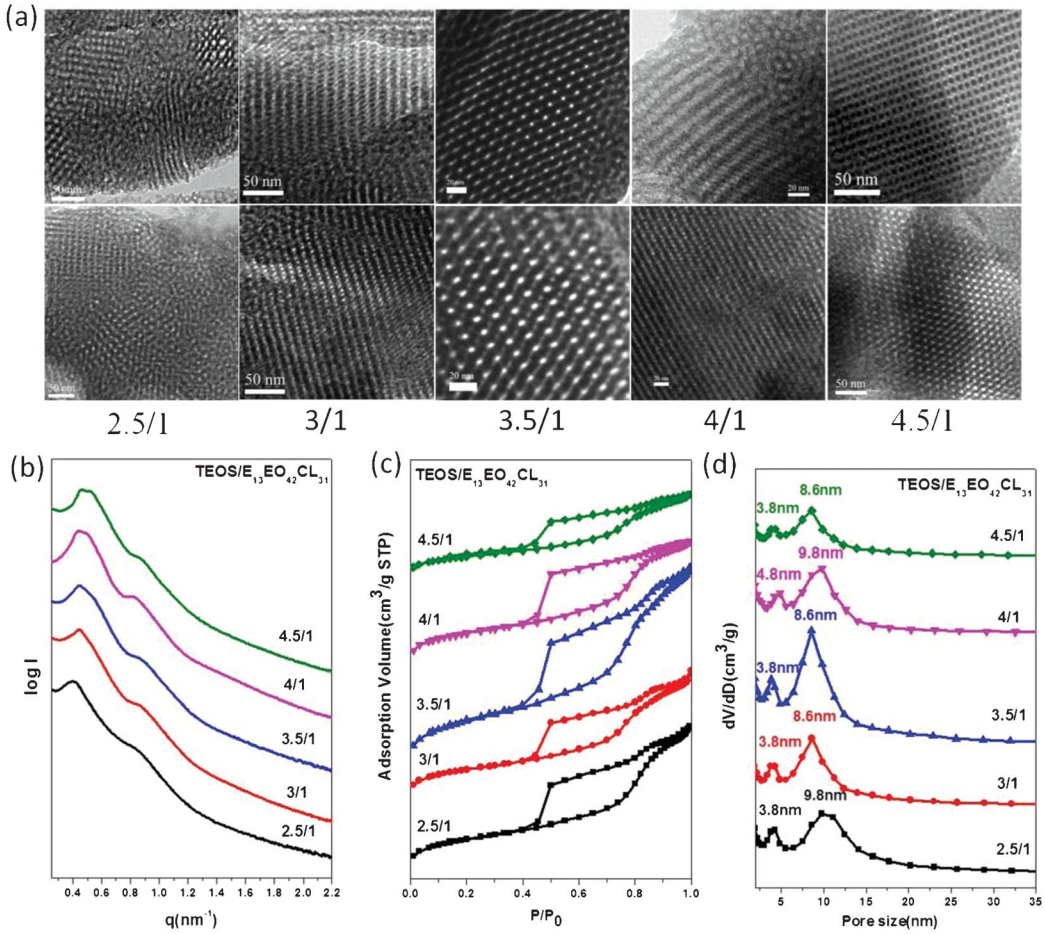

Fig. 8 (a) TEM images, (b) SAXS patterns, (c) N_2 adsorption–desorption isotherms, and (d) pore size distribution curves of mesoporous silicas templated by $E_{13}EO_{42}CL_{31}$ at TEOS-to-$E_{13}EO_{42}CL_{31}$ weight fractions of 2.5 : 1, 3.0 : 1, 3.5 : 1, 4 : 1, and 4.5 : 1.

ical mesostructure upon increasing the TEOS-to-template weight fraction. Thus, the TEOS content was insufficient to include the self-assembly system at low TEOS-to-template weight fractions, forming two kinds of mesopores: spherical pores (resulting from PE segments) and cylindrical pores (resulting from PCL segments).

In a previous study,[21] we analyzed the mesostructures of hierarchical mesoporous silicas templated by $E_{13}EO_{42}CL_{31}$ at a specific TEOS-to-template weight fraction of 3.5 : 1. The PCL segment of the template $E_{13}EO_{42}CL_{31}$ is longer than that of $E_{13}EO_{42}CL_9$; thus, as the volume fraction of the PCL block increased, the morphology of the mesoporous silicas transformed from "alternate *BCC*" (template: $E_{13}EO_{42}CL_9$) to "tetragonal cylinder alternated with *FCC*" (template: $E_{13}EO_{42}CL_{31}$). Herein, we controlled the TEOS-to-template weight fractions at 2.5 : 1 (E3T25), 3 : 1 (E3T30), 3.5 : 1 (E3T35), 4 : 1 (E3T40), and 4.5 : 1 (E3T45) and investigated the phase changes through TEM (Fig. 8a), SAXS (Fig. 8b), and BET isotherm sorption measurements (Fig. 8c and 8d). All of these mesoporous silica samples exhibited approximately the same "tetragonal cylinder alternated with *FCC*" structure, except for sample E3T25. Fig. S4, ESI† presents the characterization data of the hierarchical mesoporous silica sample (E3T35). The SAXS patterns (Fig. S4a, ESI†) reveal (111) and (311) peaks, indicating the *FCC* structure. The other peaks can be indexed to (10) and (20) reflections of the tetragonal cylinder mesostructure. Among these reflection peaks, the q value of (10) attributable to the tetragonal cylinder morphology was located at the same position as that of (110) in the *FCC* structure. TEM images and corresponding Fourier diffractograms (Fig. 4b–d) indicate that the hierarchical mesoporous silica had a high degree of periodicity when viewed from the [001], [10], and [11] directions. The BJH pore size distribution reveals that the mesoporous silica contained two distinguishable types of pores with different sizes, as calculated from the adsorption branch of isotherm curve based on the Harkins–Jura model (Fig. S4f, ESI†). Fig. 8a displays TEM images of the mesoporous silica samples E3T25 to E3T45; we observe complicated and ordered arrangements viewed from different planes, implying hierarchical and ordered structures. Taken together, the information in Fig. 8a–d reveal that the mesophase reached the best balance at a TEOS-to-template weight fraction of 3.5 : 1 and that it was difficult to shape a complete structure at the low TEOS-to-template weight fraction used to obtain E3T25.

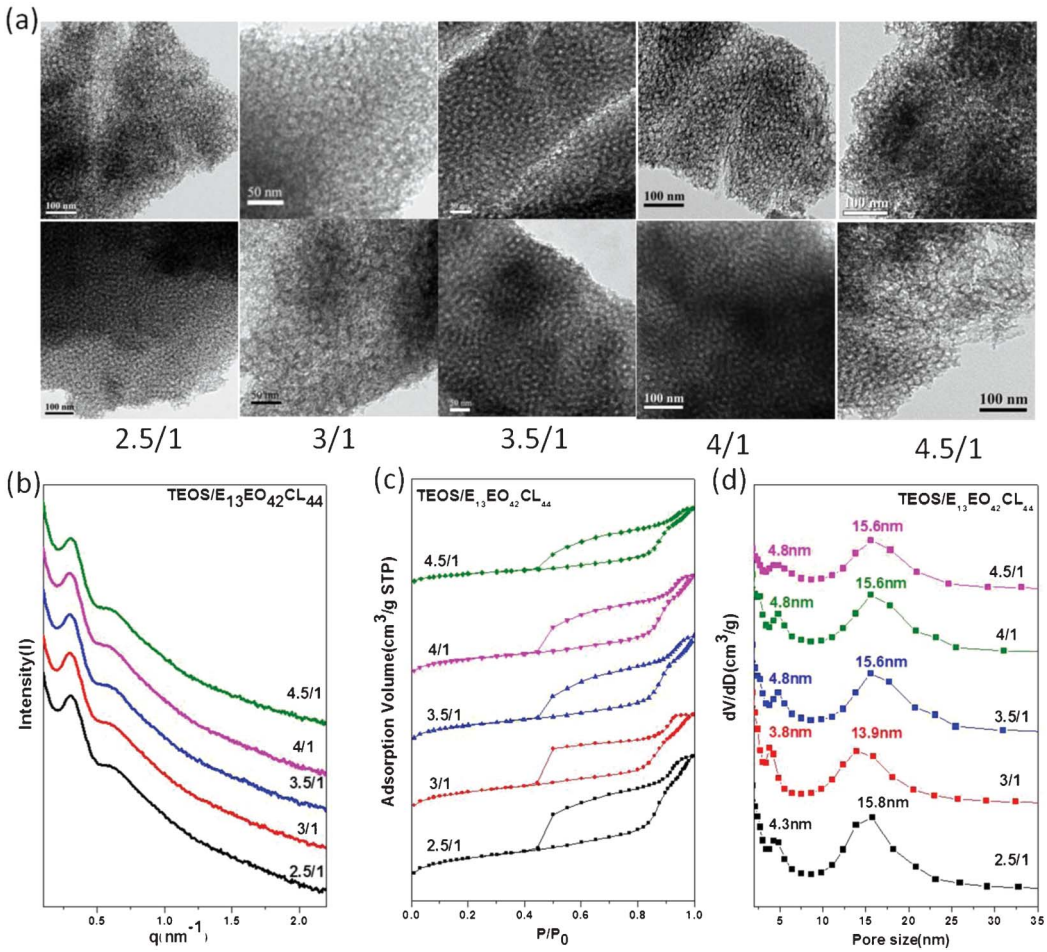

Fig. 9 (a) TEM images, (b) SAXS patterns, (c) N_2 adsorption–desorption isotherms, and (d) pore size distribution curves of mesoporous silicas templated by $E_{13}EO_{42}CL_{44}$ at TEOS-to-$E_{13}EO_{42}CL_{44}$ weight fractions of 2.5 : 1, 3.0 : 1, 3.5 : 1, 4 : 1, and 4.5 : 1

In the final part of this section, we discuss the structures formed using the ABC triblock copolymer $E_{13}EO_{42}CL_{44}$, which featured the largest PCL block among our four tested PE-PEO-PCL templates. TEM images of the mesoporous samples E4T25–E4T45 (Fig. 9a) display disordered and larger mesopores distributed by many smaller mesopores, indicating that the mesoporous silicas obviously featured two kinds of pore sizes. The SAXS patterns of these mesoporous silica samples (Fig. 9b) exhibit only tiny variations upon varying the TEOS-to-template weight fraction, suggesting that the hierarchical mesophase of these mesoporous silica samples remained almost unchanged. The N_2 sorption isotherms of the mesoporous silica samples prepared at the various TEOS-to-$E_{13}EO_{42}CL_{44}$ weight ratios exhibited (Fig. 9c) representative type-IV curves with two sharp capillary condensation steps in the relative pressure ranges from 0.85 to 0.90 and from 0.90 to 0.95, indicating multimodal pore size distributions. The two hysteresis loops of samples E4T25–E4T45 are roughly defined (Fig. 9c), with H_2-like hysteresis loops in the relative pressure (P/P_0) range between 0.45 and 0.85 and other H_2-like hysteresis loops in the range 0.90–0.97, originating from smaller spherical mesopores (PE) and larger spherical mesopores (PCL), respectively. Based on the BdB model (Fig. 9d), these mesoporous silica samples possess bimodal characteristics: a combination of smaller spherical mesopores (3.8–4.8 nm) and larger spherical mesopores (7.5–9.7 nm). Table 2 summarizes the BET surface areas, pore volumes, and BJH pore sizes of these mesoporous silica materials.

Mesoporous silicas templated by $E_{13}EO_{42}CL_{31}$ copolymers at various $HCl_{(aq)}$ contents

In a previous study, we found that the amount of $HCl_{(aq)}$ used as the catalyst during the EISA process greatly affected the morphology of the resulting mesoporous silicas for kinetic reasons.[33] Therefore, we wondered whether it would also affect the self-assembly of this TEOS/PE-PEO-PCL system. Here, we used $E_{13}EO_{42}CL_{31}$ (EEC3) as the model template and tested TEOS-to-$E_{13}EO_{42}CL_{31}$-to-HCl weight ratios of 3.5 : 1 : 0.5 (E3H05), 3.5 : 1 : 1.0 (E3H10), 3.5 : 1 : 1.5 (E3H15), and 3.5 : 1 : 2.0 (E3H20) for the fabrication of a series of mesoporous silica samples. Fig. 10a and 10b display the TEM images and SAXS patterns, respectively, of this series of mesoporous silica samples prepared at various TEOS-to-$E_{13}EO_{42}CL_{31}$-to-HCl weight ratios. The TEM images of sample E4H05 (TEOS–$E_{13}EO_{42}CL_{31}$–HCl = 3.5 : 1 : 0.5) reveal a disordered spherical pore morphology, implying that this low

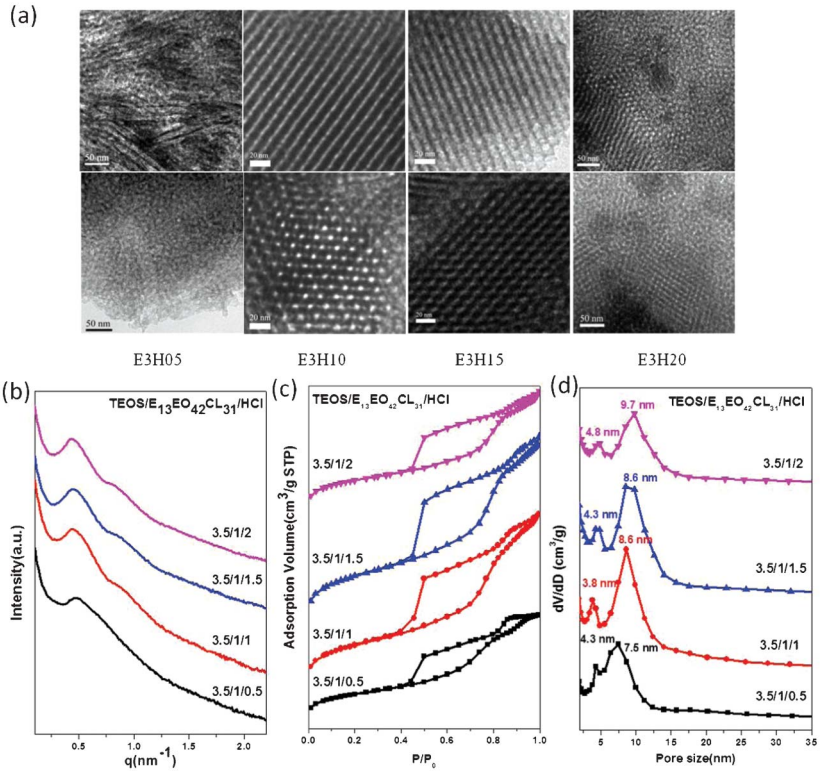

Fig. 10 (a) TEM images, (b) SAXS patterns, (c) N_2 adsorption–desorption isotherms, and (d) pore size distribution curves of mesoporous silicas templated by $E_{13}EO_{42}CL_{31}$ at TEOS-to-$E_{13}EO_{42}CL_{31}$-to-$HCl_{(aq)}$ weight fractions of 3.5 : 1 : 0.5, 3.5 : 1 : 1.0, 3.5 : 1 : 1.5, and 3.5 : 1 : 2.0.

$HCl_{(aq)}$ content led to slow rates of TEOS hydrolysis and condensation, meaning that the self-assembling system (silica precursor and PE-PEO-PCL) had sufficient time to arrange, but unfortunately it also meant that the hydrolysis and condensation of TEOS were incomplete, leading to a disordered structure. Consistent with the TEM images, the SAXS pattern of sample E4H05 displays a relatively broad scattering peak (Fig. 10b). For samples E4H10 and E4H15, the amounts of $HCl_{(aq)}$ provided the perfect balance between the rates of hydrolysis and condensation of TEOS (Fig. 10a and 10b). The sample (E4H20) prepared at the highest $HCl_{(aq)}$ content possessed a disordered hierarchical mesostructure, again due to the excessive $HCl_{(aq)}$ causing the rates of hydrolysis and condensation of TEOS to be too fast, giving the system insufficient time to self-assemble (Fig. 10a and 10b). All of the mesoporous silica samples prepared at the different TEOS-to-$E_{13}EO_{42}CL_{31}$-to-HCl weight ratios displayed typical type-IV isotherms in their N_2 adsorption/desorption curves. Fig. 10c reveals that all of these samples featured two hysteresis loops in the relative pressure (P/P_0) ranges 0.45–0.75 and 0.85–0.95; furthermore, the second loop (0.85–0.95) transformed from an H_2-like hysteresis loop to an H_1-like hysteresis loop upon increasing the $HCl_{(aq)}$ content, suggesting that the larger mesopores transformed from spherical pores to cylindrical pores. The pore size distributions of these mesoporous silica samples (Fig. 10d), determined on the basis of the Harkins–Jura model, tended to increase upon increasing the amount of $HCl_{(aq)}$. Table 3 provides further detail regarding the textures of these materials.

Mesoporous silicas templated by different PE-PEO-PCL copolymers at a constant TEOS-to-template weight ratio

In our previous research, we utilized an ABC type triblock copolymer $E_{13}EO_{42}CL_{31}$ as single template to fabricate the mesoporous silica with bimodal pore size distributions, this is the first time to use the triblock copolymer that possessed unique connected sequence of hydrophobic segment-hydrophilic segment-hydrophobic segment. Which unusual compo-

Table 3 Textural properties of mesoporous silica samples templated by PE-PEO-PCL at various TEOS-to-PE-PEO-PCL-to-$HCl_{(aq)}$ weight fractions

Sample	d (nm)	Pore size (nm)	S_{BET} ($m^2\ g^{-1}$)	S_M ($m^2\ g^{-1}$)	Pore volume ($cm^3\ g^{-1}$)	Micropore volume ($cm^3\ g^{-1}$)	TEOS/$E_{13}EO_{42}CL_{31}$/HCl
E3H05	12.8	4.3; 7.5	392	73	0.56	0.03	3.5 : 1 : 0.5
E3H10	13.8	3.8; 8.6	588	88	0.91	0.035	3.5 : 1 : 1
E3H15	13.8	4.3; 8.6	764	190	1.03	0.082	3.5 : 1 : 1.5
E3H20	15.7	4.8; 9.7	477	128	0.65	0.056	3.5 : 1 : 2

sition induced the two separate hydrophobic domains, subsequently resulting into two separate mesopores after EISA, hydrothermal treatment and calcinations. However, the key point of the previous paper is merely regarding to the new and simple method of fabrication of hierarchical mesoporous silicas, even further preparation of different hierarchical mesoporous materials by the special and convenient way. In this manuscript, we synthesized four kinds of triblock copolymer PE-PEO-PCL with increasing PCL segment length ($E_{13}EO_{42}CL_9$, $E_{13}EO_{42}CL_{18}$, $E_{13}EO_{42}CL_{31}$, and $E_{13}EO_{42}CL_{44}$), to prepare various hierarchical mesoporous silica under different prepared condition such as TEOS-to-template and HCl-to-template weight ratio, to collect all the phase behaviors of this kinds of unique ABC type template and furthermore, to find more possibility of regulating the pore structure or the pore size of hierarchical mesoporous silicas by tuning the segment length, TEOS amounts or $HCl_{(aq)}$ amounts.

Diblock copolymers can form many different well-defined, self-assembled nanostructures in the bulk state, including lamellar, gyroid, hexagonally packed cylinders, and spherical structures.[6–9] The formation of these structures results from the presence of two immiscible polymer chains connected by covalent bonds. The structures formed depend on the relative volume fractions of the blocks, the total degree of polymerization, and the Flory–Huggins interaction parameter.[6–9] Similar to the diblock copolymer system, for ABC triblock copolymer, the variable hydrophobic PCL segment of PE-PEO-PCL could also transfer the morphology from sphere to cylinder with the gradually increasing volume fraction (or molecular weight of PCL segment). Because the morphologies of mesoporous silicas were greatly affected by the molecular weight of the templating block copolymer, due to variations in volume fraction, during the EISA process in our previous study,[32] Here we also investigated the phase behavior of mesoporous silicas templated by $E_{13}EO_{42}CL_9$ (EEC1), $E_{13}EO_{42}CL_{18}$ (EEC2), $E_{13}EO_{42}CL_{31}$ (EEC3), and $E_{13}EO_{42}CL_{44}$ (EEC4), each with a different molecular weight of PCL in the PE-PEO-PCL triblock copolymer, at a constant TEOS content (TEOS-to-PE-PEO-PCL weight ratio of 3.5 : 1). The diverse hierarchical mesoporous silica samples that we obtained exhibited distinct morphologies, as observed through TEM and SAXS measurement (Fig. 11a and 11b). The mesoporous silica sample templated by EEC1 featured a clear and unusual "alternate *BCC*" structure. Among the four tested copolymers, EEC1 had the shortest hydrophobic PCL segment; therefore, it led to a spherical pores (resulting from PE segment) alternate with another spherical pores (resulting from PCL segment) ordered morphology. The hierarchical mesoporous silica sample templated by EEC3 displayed the interesting "tetragonal cylinder alternated with *FCC*" nanostructure; the PE segment was again responsible for the spherical substructure, but the PCL segment induced a transformation to the tetragonal cylinder substructure, due to expansion of the volume fraction of the PCL domain. When we used EEC2 as the template, TEM images and the SAXS pattern revealed a disordered nanostructure because the volume fraction of the PCL domain was

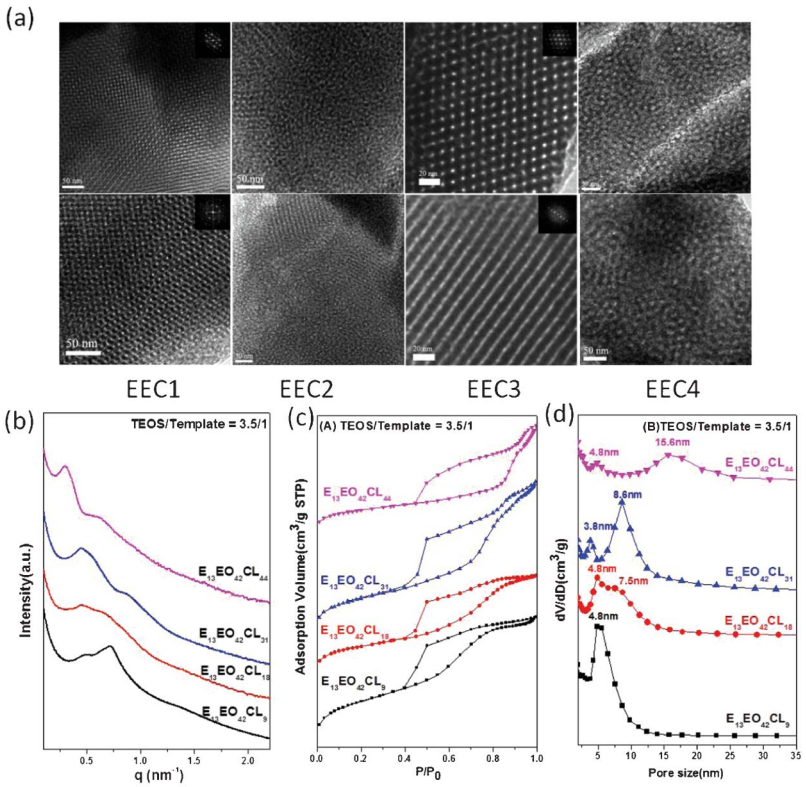

Fig. 11 (a) TEM images, (b) SAXS patterns, (c) N_2 adsorption–desorption isotherms, and (d) pore size distribution curves of mesoporous silicas templated by various PE-PEO-PCL copolymers at a TEOS-to-$EO_{114}CL_{20}$ weight fraction of 3.5 : 1.

Table 4 Textural properties of mesoporous silica samples templated by PE-PEO-PCL with various PCL molecular weights at the same TEOS-to-PE-PEO-PCL ratio

Sample	d (nm)	Pore size (nm)	S_{BET} ($m^2\ g^{-1}$)	S_M ($m^2\ g^{-1}$)	Pore volume ($cm^3\ g^{-1}$)	Micropore volume ($cm^3\ g^{-1}$)	TEOS/Template
$E_{13}EO_{42}CL_9$	12.6	4.8	795	182	0.82	0.078	3.5 : 1
$E_{13}EO_{42}CL_{18}$	13.9	4.8; 7.5	478	99	0.6	0.042	3.5 : 1
$E_{13}EO_{42}CL_{31}$	14	3.8; 8.6	588	88	0.91	0.035	3.5 : 1
$E_{13}EO_{42}CL_{44}$	21	4.8; 15.6	485	202	0.69	0.091	3.5 : 1

between those of EEC1 and EEC3; in other words, the mesophase that resulted from EEC2 is the transition state between those that originated when using EEC1 and EEC3 as templates. A further increase in the PCL length in PE-PEO-PCL to template EEC4 resulted in the ordered mesostructure being destroyed, due to over-expansion of the PCL domain (Fig. 11a and 11b); that is, the increase in the PCL volume fraction caused in the structure to move away from the ordered area of the mesophase diagram. Furthermore, according to the positions of the first-order scattering peaks in the SAXS pattern, the average spacing between the neighboring microdomains, corresponding to the size of the mesoporous domains, systemically increased upon increasing the PCL molecular weight in the PE-PEO-PCL triblock copolymers. The N_2 sorption isotherms of the hierarchical mesoporous silicas appeared as representative type-IV curves with two sharp capillary condensation steps (Fig. 11c). The mean pore sizes measured from the adsorption branch clearly revealed two kinds of mesopores (Fig. 11d). The smaller mesopores, attributable to the PE segments, remained almost unchanged, whereas the larger ones, attributable to the PCL segments, increased upon increasing the molecular weight of the PCL block in the triblock copolymer. Table 4 lists the two kinds of mesopore sizes, the surface areas, pore volumes, and other textural properties as measured through BET and SAXS analyses.

Conclusions

In this study, we synthesized a series of PE-PEO-PCL triblock copolymers–$E_{13}EO_{42}CL_9$, $E_{13}EO_{42}CL_{18}$, $E_{13}EO_{42}CL_{31}$, and $E_{13}EO_{42}CL_{44}$–with PCL segments of four different molecular weights for fabrication of hierarchical mesoporous silicas through simple ROP. Because the diblock copolymer PE-PEO is commercially available, this synthetic strategy is potentially scalable. The unusual arrangement of the three block of these special PE-PEO-PCL copolymers–comprising one hydrophilic segment and two hydrophobic segments, with the latter situated at the two termini–resulted in particular hierarchical structures for the resulting mesoporous silicas: an ''alternate *BCC*'' structure when using $E_{13}EO_{42}CL_9$ as the template and a ''tetragonal cylinder alternated with *FCC*'' structure when using $E_{13}EO_{42}CL_{31}$. Furthermore, we also investigated the phase behavior of the hierarchical mesoporous silicas with respect to (i) the TEOS-to-template weight ratio (from the point of view of the effect on the phase diagram), (ii) the HCl-to-$E_{13}EO_{42}CL_{31}$ weight ratio at a constant TEOS content (from a kinetic outlook), and (iii) the nature of the PE-PEO-PCL template at a constant TEOS-to-template weight ratio (from the viewpoint of the effect of the volume fraction of the PCL segment). The strategy that fabrication of hierarchical mesoporous silicas templated by single structure directing agent PE-PEO-PCL with unusual composition provide potential outlook due to the tunable molecular weight of unique template PE-PEO-PCL. In our cases, two special mesoporous silicas (''alternate *BCC*'' and ''tetragonal cylinder alternated with *FCC*'') with bimodal pore size distribution were obtained at the specific molecular weight of lab-made PE-PEO-PCL. In the future, we could apply the method to the other triblock copolymer, it would be the important progress in both of academic and industrious aspects.

Acknowledgements

This study was supported financially by the National Science Council, Taiwan, Republic of China, under contracts NSC-100-2221-E-110-029-MY3 and NSC-101-2628-E-110-003.

References

1 D. B. Kuang, T. Brezesinski and B. Smarsly, *J. Am. Chem. Soc.*, 2004, **126**, 10534.
2 T. Sen, G. J. T. Tiddy, J. L. Casci and M. W. Anderson, *Chem. Mater.*, 2004, **16**, 2044.
3 C. G. Oh, Y. Y. Baek and S. K. Ihm, *Adv. Mater.*, 2005, **17**, 270.
4 F. S. Xiao, L. F. Wang, C. Y. Yin, K. F. Lin, Y. Di, J. X. Li, R. R. Xu, D. S. Su, R. Schlogl, T. Yokoi and T. Tatsumi, *Angew. Chem., Int. Ed.*, 2006, **45**, 3090.
5 C. Z. Yuan, B. Gao, L. F. Shen, S. D. Yang, L. Hao, X. J. Lu, F. Zhang, L. J. Zhang and X. G. Zhang, *Nanoscale*, 2011, **3**, 529.
6 O. Sel, S. Sallard, T. Brezesinski, J. Rathousky, D. R. Dunphy, A. Collord and B. M. Smarsly, *Adv. Funct. Mater.*, 2007, **17**, 3241.
7 J. G. Yu, Y. R. Su and B. Cheng, *Adv. Funct. Mater.*, 2007, **17**, 1984.
8 S. Y. Tao, J. X. Yin and G. T. Li, *J. Mater. Chem.*, 2008, **18**, 4872.
9 L. Malfatti, M. G. Bellino, P. Innocenzi and G. Soler-Illia, *Chem. Mater.*, 2009, **21**, 2763.
10 X. Du and J. He, *Nanoscale*, 2011, **3**, 3984.

11 F. Guillemot, A. Brunet-Bruneau, E. Bourgeat-Lami, T. Gacoin, E. Barthel and J. P. Boilot, *Chem. Mater.*, 2010, **22**, 2822.
12 J. Liu, S. Z. Qiao, S. B. Hartono and G. Q. Lu, *Angew. Chem., Int. Ed.*, 2010, **49**, 4981.
13 K. Na, M. Choi, W. Park, Y. Sakamoto, O. Terasaki and R. Ryoo, *J. Am. Chem. Soc.*, 2010, **132**, 4169.
14 B. Zhao and M. M. Collinson, *Chem. Mater.*, 2010, **22**, 4312.
15 P. Innocenzi, L. Malfatti and G. Soler-Illia, *Chem. Mater.*, 2011, **23**, 2501.
16 M. Xu, D. Feng, R. Dai, H. Wu, D. Y. Zhao and G. F. Zheng, *Nanoscale*, 2011, **3**, 3329.
17 B. Mandlmeier, J. M. Szeifert, D. Fattakhova-Rohlfing, H. Amenitsch and T. Bein, *J. Am. Chem. Soc.*, 2011, **133**, 17274.
18 K. Moller and T. Bein, *Science*, 2011, **333**, 297.
19 K. Na, C. Jo, J. Kim, K. Cho, J. Jung, Y. Seo, R. J. Messinger, B. F. Chmelka and R. Ryoo, *Science*, 2011, **333**, 328.
20 K. Cho, K. Na, J. Kim, O. Terasaki and R. Ryoo, *Chem. Mater.*, 2012, **24**, 2733.
21 J. G. Li, R. B. Lin and S. W. Kuo, *Macromol. Rapid Commun.*, 2012, **33**, 678.
22 J. Wei, Q. Yue, Z. K. Sun, Y. H. Deng and D. Y. Zhao, *Angew. Chem., Int. Ed.*, 2012, **51**, 6149.
23 X. H. Zhang, Y. A. Li and C. B. Cao, *J. Mater. Chem.*, 2012, **22**, 13918.
24 T. H. Epps, T. S. Bailey, R. Waletzko and F. S. Bates, *Macromolecules*, 2003, **36**, 2873.
25 M. Sugiyama, T. A. Shefelbine, M. E. Vigild and F. S. Bates, *J. Phys. Chem. B*, 2001, **105**, 12448.
26 Y. Matsushita, *Macromolecules*, 2007, **40**, 771.
27 S. W. Kuo, *Polym. Int.*, 2009, **58**, 455.
28 J. Y. Zhang, Y. H. Deng, J. Wei, Z. K. Sun, D. Gu, H. Bongard, C. Liu, H. H. Wu, B. Tu, F. Schuth and D. Y. Zhao, *Chem. Mater.*, 2009, **21**, 3996.
29 K. Ariga, A. Vinu, T. Yamauchi, Q. Ji and J. P. Hill, *Bull. Chem. Soc. Jpn.*, 2012, **1**, 1.
30 P. Yang, S. Gai and J. Lin, *Chem. Soc. Rev.*, 2012, **41**, 3679.
31 Z. Li, J. C. Barnes, A. Bosoy, J. F. Stoddart and J. I. Zink, *Chem. Soc. Rev.*, 2012, **41**, 2590.
32 J. G. Li and S. W. Kuo, *RSC Adv.*, 2011, **1**, 1822.
33 J. G. Li, W. C. Chen and S. W. Kuo, *Microporous Mesoporous Mater.*, 2012, **163**, 34.